university of groningen

University Medical Center Groningen

University of Groningen

Investigating the state-of-the-art in whole-body MR-based attenuation correction

Beyer, Thomas; Lassen, Martin L.; Boellaard, Ronald; Delso, Gaspar; Yaqub, Maqsood; Sattler, Bernhard; Quick, Harald H.

Published in:
Magnetic resonance materials in physics biology and medicine

DOI:
10.1007/s10334-015-0505-4

IMPORTANT NOTE: You are advised to consult the publisher's version (publisher's PDF) if you wish to cite from it. Please check the document version below.

Document Version
Publisher's PDF, also known as Version of record

Publication date:
2016

Link to publication in University of Groningen/UMCG research database

Citation for published version (APA):
Beyer, T., Lassen, M. L., Boellaard, R., Delso, G., Yaqub, M., Sattler, B., & Quick, H. H. (2016). Investigating the state-of-the-art in whole-body MR-based attenuation correction: an intra-individual, inter-system, inventory study on three clinical PET/MR systems. *Magnetic resonance materials in physics biology and medicine*, *29*(1), 75-87. https://doi.org/10.1007/s10334-015-0505-4

Copyright
Other than for strictly personal use, it is not permitted to download or to forward/distribute the text or part of it without the consent of the author(s) and/or copyright holder(s), unless the work is under an open content license (like Creative Commons).

The publication may also be distributed here under the terms of Article 25fa of the Dutch Copyright Act, indicated by the “Taverne” license. More information can be found on the University of Groningen website: https://www.rug.nl/library/open-access/self-archiving-pure/taverne-amendment.

Take-down policy
If you believe that this document breaches copyright please contact us providing details, and we will remove access to the work immediately and investigate your claim.

Downloaded from the University of Groningen/UMCG research database (Pure): http://www.rug.nl/research/portal. For technical reasons the number of authors shown on this cover page is limited to 10 maximum.

Download date: 13-02-2023

Magn Reson Mater Phy (2016) 29:75–87
DOI 10.1007/s10334-015-0505-4

RESEARCH ARTICLE

Investigating the state-of-the-art in whole-body MR-based attenuation correction: an intra-individual, inter-system, inventory study on three clinical PET/MR systems

Thomas Beyer[1] · Martin L. Lassen[1] · Ronald Boellaard[2,8] · Gaspar Delso[3,7] · Maqsood Yaqub[2] · Bernhard Sattler[5] · Harald H. Quick[4,6]

Received: 6 July 2015 / Revised: 21 September 2015 / Accepted: 23 October 2015 / Published online: 6 January 2016
© ESMRMB 2015

Abstract
Objective We assess inter- and intra-subject variability of magnetic resonance (MR)-based attenuation maps (MRμMaps) of human subjects for state-of-the-art positron emission tomography (PET)/MR imaging systems.
Materials and methods Four healthy male subjects underwent repeated MR imaging with a Siemens Biograph mMR, Philips Ingenuity TF and GE SIGNA PET/MR system using product-specific MR sequences and image processing algorithms for generating MRμMaps. Total lung volumes and mean attenuation values in nine thoracic reference regions were calculated. Linear regression was used for comparing lung volumes on MRμMaps. Intra- and inter-system variability was investigated using a mixed effects model.
Results Intra-system variability was seen for the lung volume of some subjects, ($p = 0.29$). Mean attenuation values across subjects were significantly different ($p < 0.001$) due to different segmentations of the trachea. Differences in the attenuation values caused noticeable intra-individual and inter-system differences that translated into a subsequent bias of the corrected PET activity values, as verified by independent simulations.
Conclusion Significant differences of MRμMaps generated for the same subjects but different PET/MR systems resulted in differences in attenuation correction factors, particularly in the thorax. These differences currently limit the quantitative use of PET/MR in multi-center imaging studies.

Keywords Combined PET/MR · MR-based attenuation correction · Whole-body hybrid imaging · Reproducibility · Accuracy

✉ Thomas Beyer
thomas.beyer@meduniwien.ac.at

Ronald Boellaard
r.boellaard@umcg.nl

1 Center for Medical Physics and Biomedical Engineering, General Hospital Vienna, Medical University of Vienna, Waehringer Guertel 18-20/4L, 1090 Vienna, Austria

2 Department of Radiology and Nuclear Medicine, VU University Medical Center, Amsterdam, The Netherlands

3 Department of Medical Imaging, University Hospital of Zurich, Zurich, Switzerland

4 Institute of Medical Physics, University of Erlangen-Nürnberg, Erlangen, Germany

5 Department of Nuclear Medicine, University Hospital Leipzig, Leipzig, Germany

6 High Field and Hybrid MR Imaging, University Hospital Essen, Essen, Germany

7 GE Healthcare, Waukesha, WI, USA

8 Department of Nuclear Medicine and Molecular Imaging, University Medical Centre Groningen, Groningen, The Netherlands

Introduction

Combined PET/MR imaging was introduced clinically in 2006 when a prototype, combined 3-Tesla (T) MR imaging system with a fitted PET detector ring was first presented for simultaneous PET/MR imaging of the head [1]. Three major vendors have since proposed whole-body systems for simultaneous or sequential PET/MR imaging [2–4]. All whole-body PET/MR systems available today combine a 3T MR imaging with a whole-body PET system. Unlike in combined PET/CT systems, no transmission source is available for measurements of tissue attenuation. Therefore, alternative methods for MR-based attenuation correction (MR-AC) must be used for PET/MR imaging.

Several approaches have been proposed to derive computed tomography (CT)-like attenuation coefficients (μ) from the available MR images [5]. Standard methods implemented today employ either a dedicated T1-weighted (T1w) or a Dixon MR image acquisition, followed by an MR image segmentation into three or four tissue classes, none of which corresponds to bone. Imaging bone is a challenge for MR and, therefore, estimating bone in the context of acceptably short MR imaging times has not been realized yet in whole-body MR imaging [6]. The lack of bone tissue representation in MR-based attenuation maps (MRμMaps), however, has been identified as a source of visual and quantitative bias in PET images reconstructed after MR-AC [7–10].

In addition to the underestimation of attenuation coefficients from standard MR-AC, the repeatability of MRμMaps estimations has been identified as a key challenge for the adoption of PET/MR in clinical routine [4, 6]. High repeatability and reproducibility of MRμMaps, however, is key for single-center studies with individual patients in follow-up, for imaging studies with multiple patients and for multi-center studies using different PET/MR systems.

In PET and PET/CT imaging, the use of specific phantoms is the method of choice for acceptance testing, periodic quality control measures as well as initiation procedures for standardized single- or multi-center imaging protocols [11–13]. Phantoms can be standardized to specific imaging needs; they can be manufactured with high quality and reproducibility and, finally, made available to many users at different sites for performing comparative and repetitive studies. However, PET-type phantoms are limited for the evaluation of MRμMaps due to their inherent inability to depict MR imaging characteristics of human tissue and tissue distribution [14].

In view of the shortcomings of phantom-based system evaluation and assessment of the quality of MR-AC, alternative methods for investigating MR-AC implementations must be found. This study presents an approach using a group of different-sized volunteers, subject to test–retest imaging in three whole-body PET/MR systems as a simple, initial quality survey method in single-center and multi-center settings.

Materials and methods

PET/MR systems and standard MR-AC methods

This study was performed between September 2013 and April 2014 and included three types of whole-body PET/MR systems available during that period (Fig. 1): Siemens Biograph mMR [2], Philips Ingenuity TF PET/MR [3] and GE SIGNA PET/MR (CE label and FDA approval pending at time of investigation) [15]. All PET/MR systems were in working condition at the time of the study and successfully passed acceptance and quality testing. At the time of the investigations, all systems were operational and equipped with the following system software: syngo VB18P (Biograph mMR), PET/MRI Release 3.2.2 (Ingenuity TF) and MP24.0_EA_1350 (SIGNA).

The PET/MR systems evaluated in this study had the following standard methods for MR-AC implemented (Table 1).

Biograph mMR A dedicated Dixon-VIBE sequence for MR-AC in coronal orientation precedes PET/MR measurements for each bed position. In- and opposed-phase images are recomposed into fat and water images, and segmented into four tissue classes (air, lung, fat and soft tissue), each with a fixed attenuation value for 511 keV photons [16]. The attenuation maps were acquired using a set of radiofrequency (RF) surface coils: 16-channel RF head/neck coil, 24-channel RF spine array coil and 6-channel body matrix RF coils.

Ingenuity TF Transverse T1w-GE MR images are acquired and segmented into three tissue classes (air, lung and soft tissue) with fixed attenuation values in each class. MR-AC acquisitions were performed using the built-in RF transmit/receive body coil (Q-body).

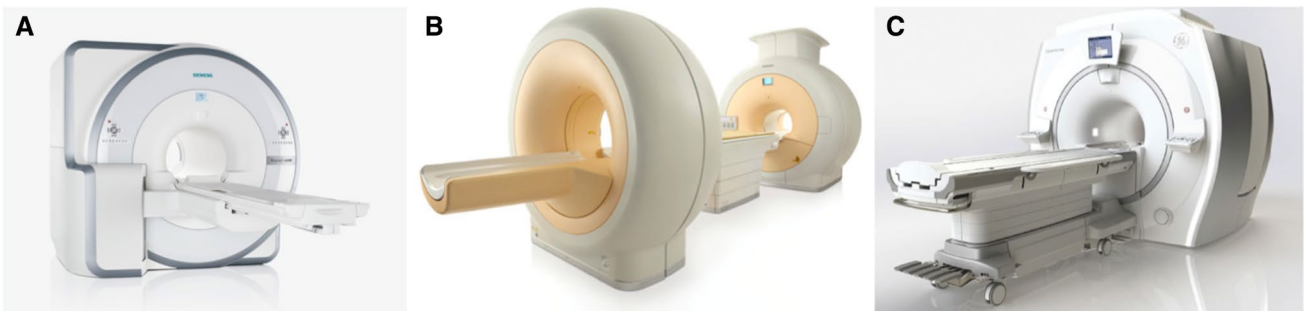

Fig. 1 Whole-body PET/MR hybrid imaging systems investigated in this study: Siemens Biograph mMR (**a**), Philips Ingenuity TF (**b**) and GE SIGNA (**c**)

Table 1 Overview of MR imaging parameters for standard MR-AC procedure and MR-AC algorithms, as well as typical MR-based attenuation values (cm-1)

	Biograph mMR Siemens	Ingenuity TF Philips	SIGNA GE
Software version	VB18P	Release 3.2.2	EMP24.0_EA_1350
AC sequence	Dixon VIBE	Multi-stack spoiled T1w GE	LAVA-FLEX
TR/TE (ms)	3.6/2.46	4.1/2.3	4.0/1.7
Flip (°)	10	10	5
Matrix (in-plane)	128 × 192 2.6 × 2.6 (mm)	144 × 144 4 × 4 (mm)	256 × 128 4.69 × 4.69 (mm)
Slice (mm)	2.6	4	2.8
Orientation	HFS–coronal	HFS–transversal	HFS–axial
Coils	Surface RF coils	Built-in body RF coil	Built-in body RF coil
Breath-hold	Yes (thorax) No (elsewhere)	No	No
Scan time (s) per bed	18	24	18
Bed positions to cover head to thighs	5	10–11	5
Tissue classes	4	3	5
Tissue types	Air, lung, soft tissue, fat	Air, lung, soft tissue	Air, lung, soft tissue, fat, bone
Linear attenuation values [cm-1] at 511 keV			
Lungs	Fixed (0.0240)	Fixed (0.0219)	Fixed (0.0180)
Soft tissue	Fixed (0.1000)	Fixed (0.0950)	Variable (0.086-0.100)
Fat	Fixed (0.0854)	NA	Variable (0.086-0.100)
Bone	NA	NA	Variable (skull: atlas-based)

HFS head first supine, *RF* radiofrequency, *TR* repetition time, *TE* echo time

SIGNA A multi-station, whole-body, three dimensional (3D), dual-echo, RF spoiled gradient recalled echo (SPGR) sequence (LAVA-FLEX) in transaxial orientation is used for MR-AC. Similar to the Dixon-based approach (Biograph mMR), water-only and fat-only images are calculated from in-phase and out-of-phase images from which MRμMaps with four tissue classes (air, lung, fat and soft tissue) are derived. The air and lung tissue classes are binary, whereas the classification between fat and soft tissue is variable: the LAVA-Flex fat/water ratio is used to obtain a weighted average of fat (0.086 cm^{-1}) and water (0.100 cm^{-1}). For the head, a CT-based atlas, including bone tissue, is co-registered to the acquired MR image. MR data were acquired with the built-in RF transmit/receive body coil.

Subjects

Informed written consent for MR-only examinations was obtained from each volunteer prior to the MR imaging study in compliance with the local institutional review board guidelines. Four healthy male subjects [mean age: 45 ± 1 years, mean body mass index (BMI): 27 ± 3] were included. During the course of this study, one subject (S4) lost over 20 % of body weight and, therefore, was rescanned [S4(s)] on the Biograph mMR and Ingenuity TF PET/MR systems.

Acquisitions

Subjects were positioned head-first supine (HFS) and arms down on the PET/MR systems by experienced on-site technologists. Each subject underwent a simulated whole-body PET/MR examination covering a standard imaging range from the top of the skull to the mid-thighs, corresponding to 5–6 bed positions for two systems (mMR, SIGNA) and 10–11 bed positions for one system (Ingenuity). Neither a PET tracer nor MR contrast was injected. PET/MR protocols were run for the part of the MR examination only. For each system vendor-specific instructions for standard MR-AC were followed: subjects were asked to hold their breath in normal expiration (mMR) or to breathe freely (Ingenuity, SIGNA) when imaging the thorax, all other body stations were acquired during free breathing (Table 1).

All subjects underwent a second, retest scan on the same day after being repositioned on the PET/MR system within 1 h. All scans were completed with a T1w-MR image sequence to obtain a high-resolution anatomical overview of all volunteers serving as a reference standard for the evaluation of correct tissue segmentation in MR-AC. T1w imaging was performed using the RF surface coils (mMR) and the Q-body RF surface coils (Ingenuity). In the SIGNA, the RF surface coils GEM 19-channel head-neck

unit, 16-channel upper and lower anterior arrays and 14-channel central posterior array were used.

Image processing

Whole-body MRμMaps were composed of overlapping single-bed attenuation maps following the standard, vendor-specific image processing (Table 1; Fig. 2). At the time of the evaluation of the attenuation maps, the SIGNA system had a non-product "released for evaluation" version of the software and, therefore, whole-body attenuation maps were composed at the vendor factory.

Data analysis

First, all MRμMaps were reviewed by two experienced imaging physicists in consensus for image artifacts, such as truncation or susceptibility-induced image distortions

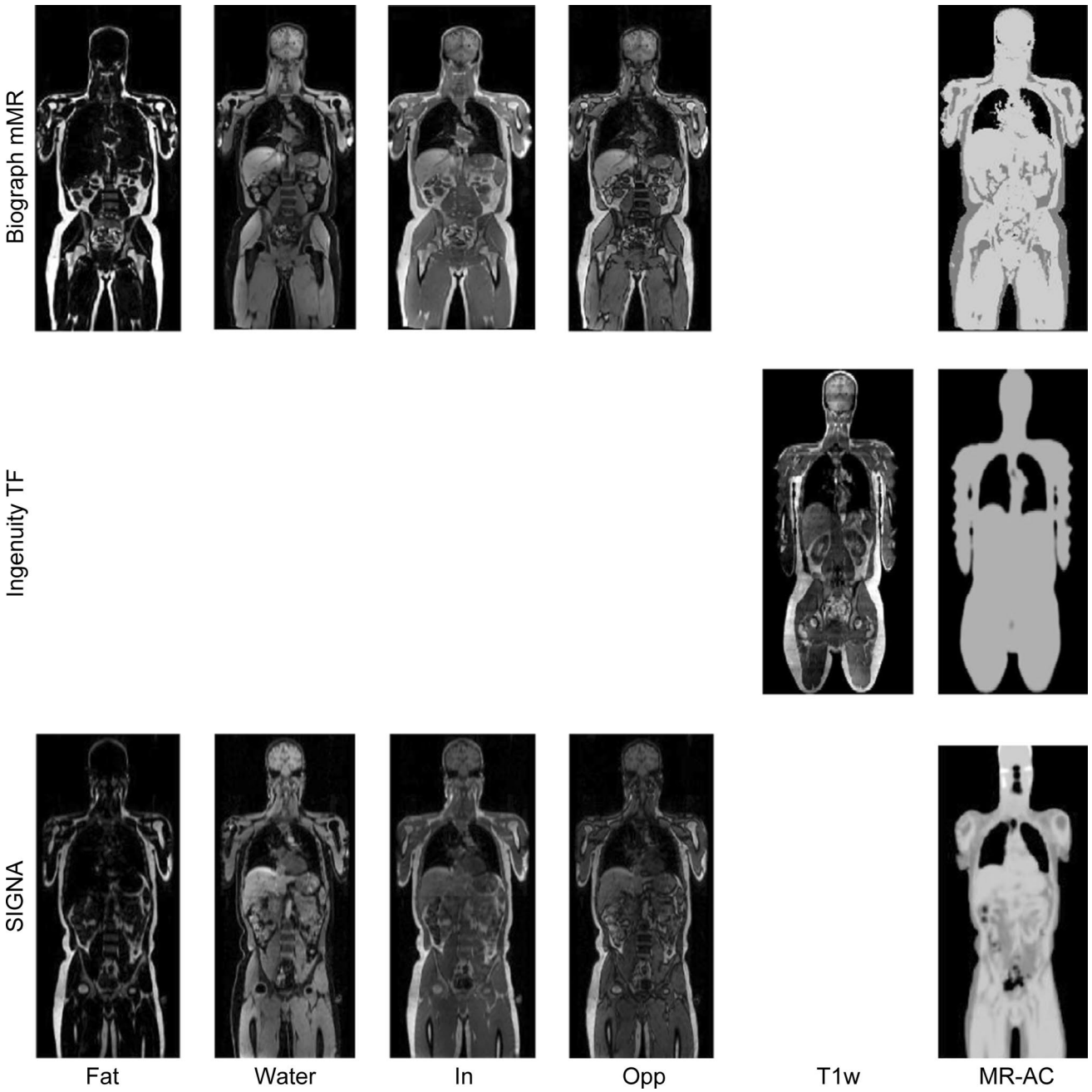

Fig. 2 Coronal MR images of subject 2 (*left*: fat, water, in-phase and opposed-phase) for deriving MR-based attenuation maps (MR-AC, right). The attenuation map for the Ingenuity TF is obtained from a stack of axial T1w-images, whereas MR-AC in the Biograph mMR and SIGNA systems is based on a Dixon and Dixon plus atlas (skull) approach, respectively

[9]. We report on the number of MR-attenuation maps with visually noticeable artifacts.

Second, for each subject, whole-body MRμMaps from test–retest scans on all three PET/MR systems were aligned to the whole-body T1w-MR images of the Biograph mMR (test) to enable subsequent analyses. Alignment was performed using an affine co-registration algorithm (Mirada Medical XD Advanced 3.6.4.8, Mirada Medical, UK). Resampling of all aligned MRμMaps was performed according to the matrix and voxel size of the mMR attenuation maps. For each subject and matched attenuation map, the total lung volume was estimated from a seed-point growing algorithm within Mirada Medical XD. Upper and lower threshold values for the seed-point algorithm were defined by using the vendor-specific attenuation values for the lungs (Table 1). Individual adjustments were necessary to ensure a full segmentation of the lungs, in case of visually confirmed incorrect separation of lungs and soft tissue. These thresholds were accessed by visual inspection of the MRμMaps. Linear regression of the lung volumes was analyzed in Graphpad Prism 6.04 (Graphpad Software, San Diego, CA, USA).

Third, nine reference regions were defined for each subject as volumes of interest (VOIs) in the lungs, mediastinum, liver and spine on the T1w image. These VOIs were copied to all matched MRμMaps (Fig. 3). Lung attenuation values were determined from a total of six VOIs (Fig. 3b); four VOIs in the upper and lower lungs were averaged to represent the mean attenuation value in the apical regions, while the average of the remaining two VOIs represented the attenuation in the center region of the lungs. For each subject and VOI mean [± standard deviation (±SD)] attenuation values are reported. Attenuation values were averaged across subjects and PET/MR systems, and compared to the attenuation values set forth by the vendors. Calculated attenuation coefficients were analyzed with mixed effects models (MEMs; *R*, the GNU Project) employing two-sided parametric tests with a threshold value of $p < 0.05$. Of note, a MEM is a powerful statistical tool that can provide *p*-values of repeated measurement studies with missing datasets. Here, we consider any changes of the intra-subject variability of MRμMaps in a scan–rescan test to be representative of such changes during follow-up imaging of the same patient with a given PET/MR system. In addition, inter-system variability of MRμMaps of the same subjects are indicative of changes of attenuation values during follow-up of patients using different PET/MR systems. Lastly, comparisons of intra- and inter-system variability in this study may reflect the variability seen in multi-center trials with different PET/MR systems.

Fourth, transverse projections of the MR-based attenuation maps [projection-based linear attenuation coefficients

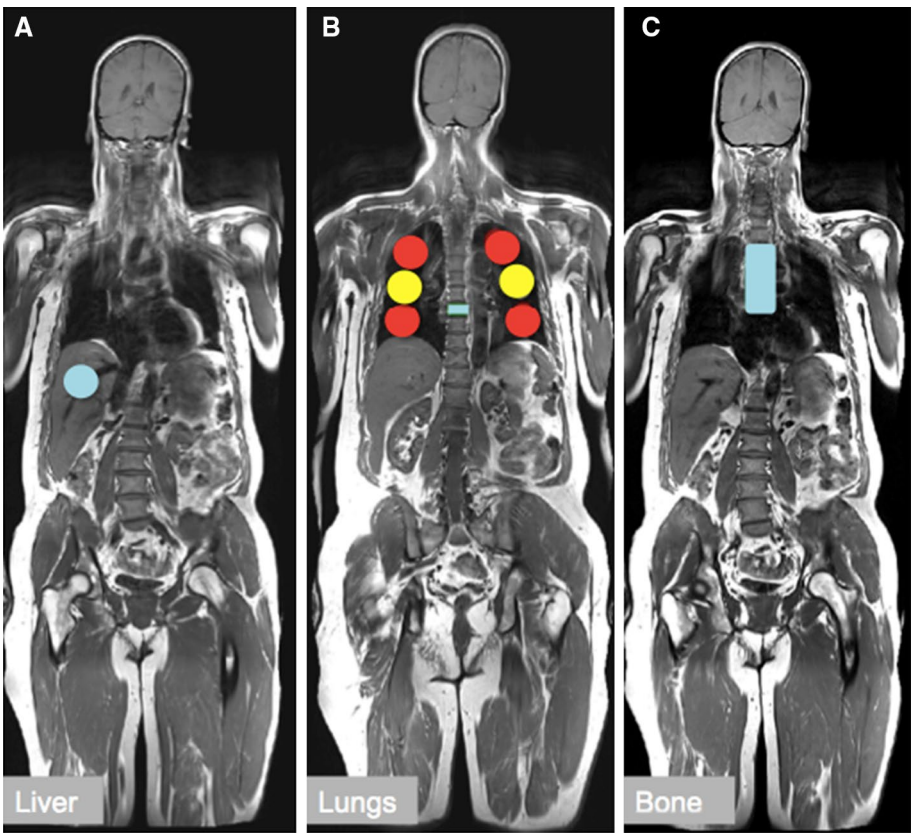

Fig. 3 Reference VOIs on coronal T1w-MR image of subject 1: **a** 3-cm spherical VOI placed in the liver, **b** upper (*red*), lower (*red*) and central (*yellow*) lung VOIs (all 3-cm spherical) and spinal column VOI (T4 segment), and **c** mediastinum VOI

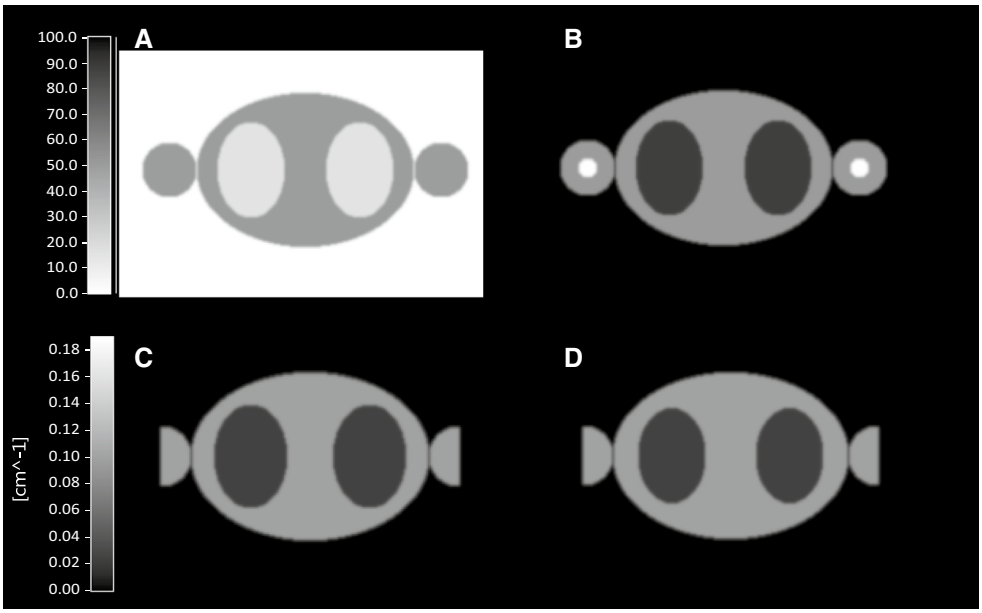

Fig. 4 Central axial view of mathematical 'thorax' phantom (torso with lung inserts and bi-lateral arms) to estimate PET activity bias from variable attenuation maps: **a** uniform PET activity distribution with 1/3 background activity placed in the lungs; **b** corresponding ATN (attenuation) map with true soft tissue, lung and bone attenuation coefficients assigned, true; **c** truncated MR-based ATN, MRAC; and **d** truncated MR-based ATN with reduced lung volume (thMRAC), thus, simulating lung segmentation errors and differences in pLACs as seen in human data (Fig. 4A)

(pLACs)] were averaged across all angles in order to assess both qualitatively and quantitatively intra-individual and inter-system variability of all resulting MRμMaps. Of note, the projected image volume was limited to a central 45-cm diameter data set to eliminate the influence of truncation-based distortions and focused on the thorax region. pLAC values were calculated in MatLab 7.9.0 (Mathworks, Massachusetts, USA).

Simulations

Any pertinent effects from varying MRμMaps on the quality and accuracy of PET emission images after MR-AC were assessed by means of a simulation using a geometrically simple, noise-free 'thorax' phantom. The phantom was 40 cm and 28 cm in long and short axis views, respectively, with ellipsoidal lung inserts and cortical bones limited to the arm regions (Fig. 4). The activity concentration in the lungs was 30 % of the soft tissue activity concentration (Fig. 4a). The corresponding attenuation map (Fig. 4b) employed a standard LAC: 0.022 cm^{-1} (lungs), 0.096 cm^{-1} (soft tissue) and 0.18 cm^{-1} (bone). Standard MR-AC was simulated by including truncation effects and by setting the attenuation coefficient of bone to that of soft tissue (Fig. 4c). As will be shown later in more detail, relative mean differences in pLAC and median lung volumes (Fig. 5a) of up to 10 % and 10–30 %, respectively, were found in the clinical data. Therefore, a third attenuation map was simulated with a 20 % smaller lung volume (Fig. 4d) such that the average pLAC for this phantom changed by 10 %.

Simulations of attenuation correction and PET image generation are similar to the methodology in Boellaard et al. [17]. In short, after defining the simulated activity distribution (mathematical 'thorax' phantom), sinogram data were generated from these images using an analytical forward projector including time-of-flight (TOF) and attenuation using the complete and correct simulated μMaps. In order to account for the differences in the TOF performance of the three PET/MR systems, the following timing resolutions were assumed: non-TOF, 650 and 325 ps, both for generating sinogram data as well as during image reconstruction, as indicated below. The simulated noise-free projection data were then reconstructed using ordered subset expectation maximization (OSEM) reconstructions without or with corresponding TOF (6 iterations, 16 subsets) to 256 × 256 transaxial images. PET images were reconstructed using three attenuation maps (μMaps): complete and correct μMaps (true), truncated MRμMaps (MRAC) and truncated MRμMaps with reduced lung volume (thMRAC). Difference maps (DiffMap) of PET images reconstructed with MRAC and thMRAC were generated with PET (true) serving as the reference.

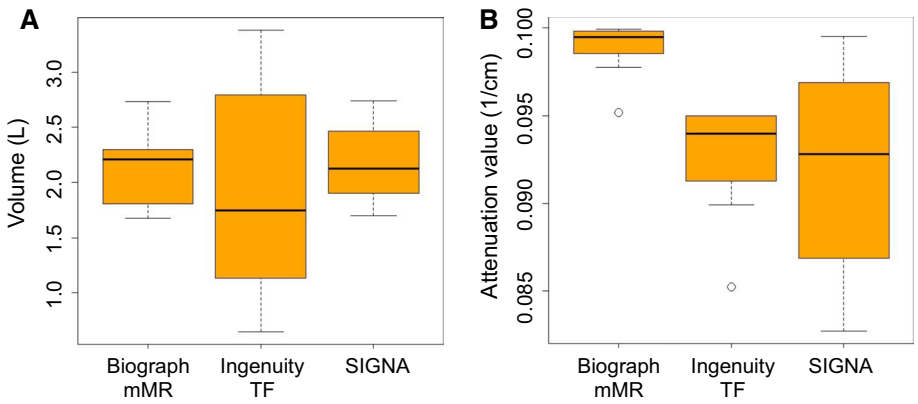

Fig. 5 *Boxplots* of system-specific lung volumes (**a**) and mediastinum attenuation values (**b**) across subjects and time points. Similar median values are seen for the lung volumes in the Biograph mMR and SIGNA systems, while the Ingenuity TF resulted in a wider spread of lung volumes (**a**). The different median attenuation values for the mediastinum reflect different degrees of segmentation of the trachea, and the different vendor-specified attenuation values for soft tissue (**b**)

Results

Human data

Three of the four subjects had repeated measurements on all three PET/MR systems (Fig. 1) following repositioning on the patient table. One subject (S4) had repeated measurements on the Biograph mMR (Fig. 1a) and Ingenuity TF (Fig. 1b) following a significant loss of body weight during the course of the study. Figure 6 shows coronal sections of MR-based attenuation maps of all four subjects scanned on the three PET/MR systems. Image comparison across subjects and PET/MR systems demonstrates a variable degree of anatomically correct representation of attenuating tissues. Also, the classification of tissues into three (Ingenuity) or four tissue classes (mMR, SIGNA) is clearly seen with the SIGNA images expressing the skull as well.

Image artifacts were observed in all MRμMaps of all subjects (Table 3). Specifically, truncation artifacts along the arms (Fig. 7a) were present in all MRμMaps of all subjects and across all systems. Artifactual air inserts in the intestines and bladder (Fig. 7b, c) were found in a significant portion of scans. The frequency, size and position of these artifacts varied with the PET/MR systems and subjects, and, thus, did not introduce systematic errors in the μMaps.

Lung volume analyses revealed large intra- and inter-system variability (Fig. 5). Figure 5a shows similar median values of the system-specific lung volumes for the mMR and SIGNA system, while for the Ingenuity TF, the median was lower with a wider percentile variation. Absolute inter-system variability of the median lung volume was 29 %. Intra-system variability was higher for the ingenuity TF system with up to 1.5 L in subject 3 (Fig. 8). In general, intra-system variability was observed to be smaller than inter-system variability for the respective subjects (Fig. 8). Based on the MEM analysis, differences in the lung volume across all subjects were independent of the subject weight ($p = 0.98$).

Table 2 lists the average attenuation values of all scans and subjects. Of note, lung attenuation values (cm^{-1}) were lower for the SIGNA system than for the other two PET/MR systems. Attenuation values in the mediastinum, liver and spinal column were highest for the Biograph mMR and similar for the other systems. For all systems, the VOI-based attenuation measurements corresponded to the expected attenuation values for the different tissue classes. Deviations were observed for the mediastinal attenuation values (Table 2). Varying degrees of intra-system variability were detected for all regions using the MEM analysis with p-values in the range of $p < 0.01$ (mediastinum) and $p = 0.97$ (lungs). Of interest, the variability of the attenuation values in the liver across the three systems was not significant ($p = 0.099$). In contrast, average attenuation values in the mediastinum across the PET/MR systems were statistically significant ($p < 0.01$, Fig. 4b).

Noticeable intra-individual and inter-system differences of the pLAC values were found for the skull, lungs and abdominal region (Fig. 9). On average, total integral attenuation values, pLAC, across the lungs of all subjects differed by up to 10 % across PET/MR systems, indicating a systematic bias from standard MR-AC in different whole-body PET/MR systems.

Simulations

Results from the simulations are presented in Fig. 10. The difference maps of the PET activity show that the use of MRμMaps may lead to substantial underestimations of up to −50 % compared with the true PET activity, in particular, in areas affected by truncation and missing bones

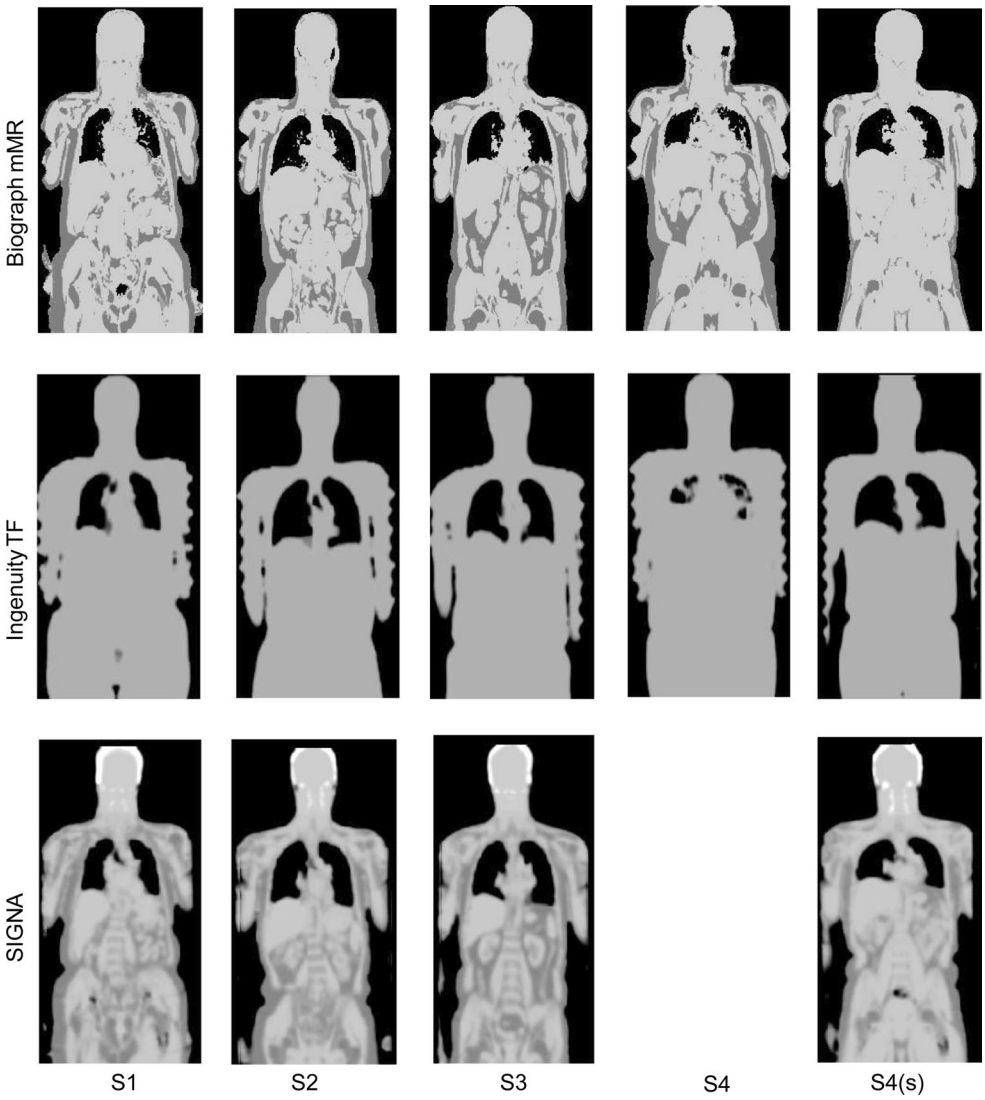

Fig. 6 Coronal sections of MR-based attenuation maps from first scan of all subjects on all three PET/MR systems. Subject 4 was scanned a second time on the Biograph mMR and Ingenuity TF system after significant weight loss (S4), as described in the Methods section. The Biograph mMR (*top*) and IngenuityTF (*middle*) yield 3- and 2-class tissue representation, respectively, while the SIGNA (*bottom*) offers additional bone tissue representation in the head

Table 2 Average MR-based LACs [cm-1] obtained from all participants

System	Subjects/scans	Lungs, apex	Lungs, center	Mediastinum	Liver	Spine
Biograph mMR	5/10	0.023 ± 0.001	0.022 ± 0.000	0.099 ± 0.001	0.1 ± 0.0	0.01 ± 0.00
Ingenuity TF	5/9	0.022 ± 0.010	0.026 ± 0.008	0.093 ± 0.003	0.095 ± 0.000	0.094 ± 0.002
SIGNA	4/8	0.019 ± 0.001	0.018 ± 0.000	0.092 ± 0.006	0.1 ± 0.0	0.097 ± 0.001

Table 3 Artifacts found in MR-AC attenuation maps generated from all three PET/MR systems

Number of scans	Truncation	Missing bone*	Bladder segmented as "air"	Intestines segmented as "air"	Lungs with "soft tissue" inserts
Biograph mMR	10/10	10/10	5/10	4/10	0/10
Ingenuity TF	9/9	9/9	3/9	3/9	3/9
SIGNA	8/8	8 (0)/8*	6/8	3/8	0/8

Multiple artifacts are only counted once per system and scan

* In all scans, the LAC of bone in the thorax/extremities were substituted by the LAC of soft tissue. The SIGNA system had skull bones introduced into the attenuation maps by using an atlas-based method (score 0 in parenthesis)

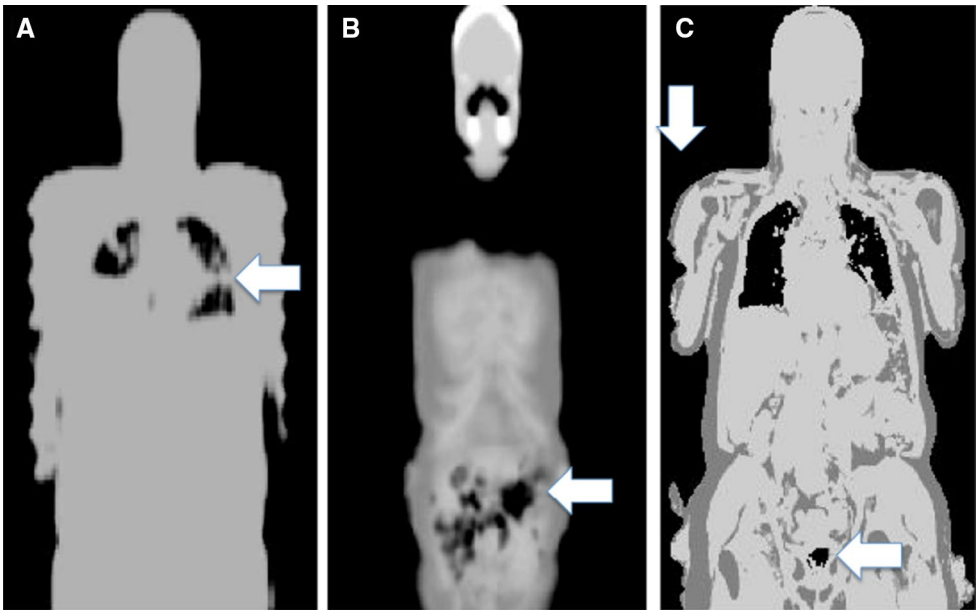

Fig. 7 Examples of typical artifacts in MR-based attenuation maps: **a** erroneous lung segmentation with soft tissue inserts (S4 in Ingenuity TF), **b**, **c** extended "air"-filled regions that may originate from susceptibility changes (S2 on SIGNA and Biograph mMR systems), and **c** truncation along the exterior of the body (S1 on Biograph mMR system)

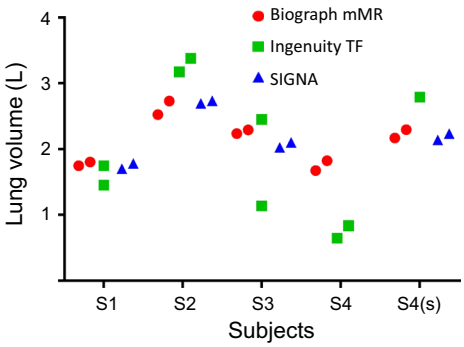

Fig. 8 Lung volumes estimated from MR attenuation maps vary across subjects and systems. Highest intra- and inter-system variability was found for S3 and, a larger subject, S4, respectively

(Fig. 10a). When reducing the lung volume (thMRAC), a large upward bias was observed along the lung boundaries, due to low attenuating lung tissue being replaced by high attenuation soft tissue in the simulated μ map (Fig. 4b, d). The net impact of incorrect lung segmentation (MRAC-thMRAC) is illustrated in Fig. 10c; in non-TOF images, over- and underestimations of PET activity are seen primarily in the lung boundaries and mediastinum, and the lungs, respectively. This pattern changes in TOF images (Fig. 10, middle and bottom row) with only a slight overestimation of 10–20 % observed across the torso.

Discussion

The aim of this study was to evaluate the quality of MR-based attenuation maps in the context of clinical, whole-body PET/MR imaging. Therefore, MR-based attenuation correction data of four subjects were acquired on three different state-of-the-art whole-body PET/MR systems. This study included test–retest imaging to address current concerns over the limited repeatability and reproducibility of MRμMaps.

Truncation and missing bone effects were the most prominent image artifacts in standard whole-body MRμMaps (Table 3). Other image distortions included tissue swap effects (i.e. inverted assignment of soft tissue and fat in the MRμMaps [18]) and issues frequently related to air-filled image volumes in the abdomen and bladder regions. Thus, our limited subject cohort supports the notion of frequently observed artifacts in MRμMaps [9].

The present study focused on standard, whole-body imaging scenarios and showed noticeable differences across subjects and systems for segmented lung volumes and tissue attenuation values (Figs. 5, 6, 8). These differences, in particular across PET/MR systems (Figs. 5b, 8), were expected since standard breathing instructions during the coverage of the thoracic region were different (Table 1): free breathing (Ingenuity, SIGNA) and normal expiration (mMR). In reality, inter- and intra-scan respiration across subjects is different, and the attenuation values of regions in the lungs and cavities have higher probability of being misclassified than areas affected less by respiration, such as the abdomen. Of note, significant differences ($p < 0.001$) were observed between subjects in the mediastinum, caused by the different delineation of the trachea on the MRμMaps (Figs. 5b, 6).

This study revealed an inter-system variability of the estimated lung volume that was, however, not significant ($p = 0.29$). Still, such differences may originate from

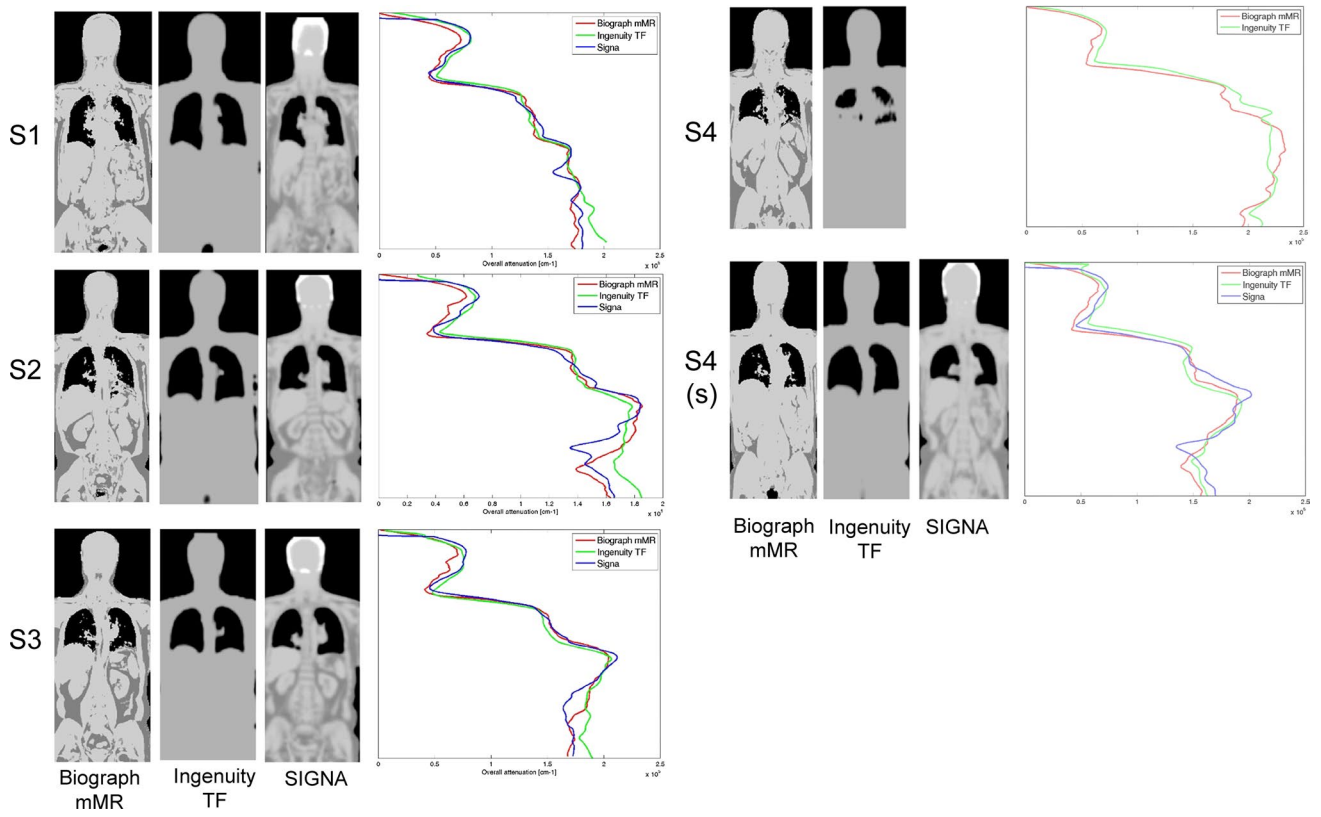

Fig. 9 MR-based attenuation maps of all subjects [S1-S4(s)] and all PET/MR systems. Attenuation maps were devoid of truncation artifacts; only data of a 45-cm central cylinder volume were used for total projections (*right*) by integrating the assigned LAC of each MR-AC map along the subject's body. *Line plots* of LAC demonstrate noticeable differences in the regions of the pelvis (up to 27%), skull (up to 25%) and lungs (up to 22%). For the SIGNA system, higher LACs in the skull region were observed due to the incorporation of cranial bone attenuation values in the MR-attenuation map (Fig. 1)

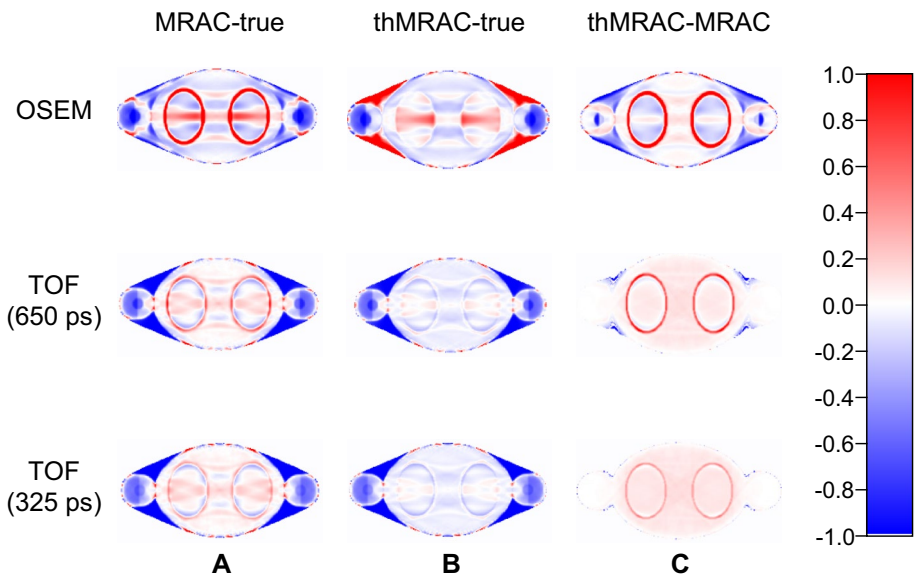

Fig. 10 Axial (normalized) difference maps of reconstructed PET images following attenuation correction with **a** with correct lung volume (MRAC-true) and **b** with 20 % smaller lung volumes (trMRAC-true) for 3 different reconstructions synonymous with the three PET/MR systems. The net impact of incorrect lung segmentation is shown in (**c**), which is the difference between (**a**) and (**b**). All images show the difference normalized to the true simulated PET activity. Of note, the PET activity bias varies with the distance from the artefact and the reconstruction method used

different levels of breath-hold during the estimation of MRμMaps and subsequent erroneous segmentation of the lungs. Respiration artifacts are further exemplified by so called "banana" artifacts, indicating a local mismatch of the vertical level of the diaphragm on MRμMaps and the average position of the diaphragm during the emission acquisition [9]. Lung segmentation errors were observed in three image volumes from the Ingenuity TF, one of which is presented in Fig. 7a [19]. These soft tissue "bars" resulted in a large reduction in the lung volume (Fig. 8, subjects S3 and S4). In summary, subject-specific repeatability was acceptable for the majority of subjects and systems, but test–retest reproducibility was limited for subjects imaged on the Ingenuity TF at the time of this study.

To further assess the impact of artifacts and assignment of different LAC values in MRμMaps on the final PET quantification, average line integrals of the total attenuation value (pLAC) projections across all angles were calculated for all scans and all subjects. The analyses revealed local differences in pLAC values of up to 27% (pelvis), 25% (skull) and 22% (lungs). These differences were introduced by the differences in the assigned tissue attenuation values (Fig. 9). Of note, this study population was limited to the evaluation of MR-based attenuation images of human subjects.

To further evaluate how variable pLAC values affect the reconstructed PET activity values, we have performed an independent simulation (Fig. 10). The simulations provide an approximate understanding of the artefacts and effects of variability of lung segmentations during MR-AC. The 20 % change in lung volume corresponds to the observed differences in median lung volumes (Fig. 5a) and pLAC values in our subjects (Fig. 9). Our simulations suggest that standardized uptake value (SUV) biases of up to +20 % may occur due to incorrect lung segmentations alone (Fig. 10). At the same time, negative biases occur due to truncation and missing bones. Figure 10 further supports the conclusion of Conti et al. [20] who reported that TOF-based image reconstructions help limit the magnitude and extent of the bias from incorrect AC.

This study is an inventory study, evaluating standard methods for MR-AC in state-of-the-art whole-body PET/MR systems as available at the time of the measurements. Implementations of MR-AC in clinical PET/MR systems today are improving steadily. Iterative algorithms [21–23] and algorithms for increasing the MR-based field of view (FOV) [24, 25] have been suggested to balance the presence and magnitude of truncation artifacts. The lack of bone attenuation information can be addressed in MR-AC of the brain by using atlas-based methods [26, 27] or by using ultra short echo time (UTE) pulse sequences [28, 29]. The most recent product software version (VB20P for Biograph mMR) now provides for an UTE-based delineation of skull bone. The implementation of an atlas-based method for whole-body MR-based AC providing continuous attenuation values for the main skeletal structure is currently under evaluation [30]. In addition, hardware components, such as RF coils, must be considered during MR-AC [31–34].

This study is a proof-of-concept and, as such, has some limitations. This includes the limited number of exclusively male subjects participating in this study that included measurements at three PET/MR sites in three European countries. The number of participants limits the statistical power of this study and increases the influence of outliers. For example, measurements on the Ingenuity TF had a comparatively high impact on the statistics. The scope of this study was, however, not to analyze which PET/MR system performed best, but to assess the repeatability of standard MRμMaps using state-of-the-art PET/MR systems. In this study, each subject served as its own control. This eliminates the need of using both male and female subjects, even though differences in the fat deposits and lung volumes are present between male and females [35]. Errors in regional attenuation coefficients and pLAC values resulting from truncation of the arms were neglected in this study. Truncation artifacts can be corrected potentially in clinical routine by deriving the outer contour of the body and arms from non-attenuation-corrected PET data [36], or by using dedicated image reconstruction methods, such as the maximum likelihood reconstruction of attenuation and activity (MLAA) method [23].

Conclusion

Significant intra-subject differences of MRμMaps derived from different state-of-the-art PET/MR systems were observed. These differences may translate into noticeable variations of PET activity distributions. The observed limitations in repeatability and reproducibility may limit the quantitative use of PET/MR in intra-subject follow-up scenarios and, more so, in multi-center imaging studies.

Acknowledgments We thank the following technologists for their assistance in collecting the data: Femke Jongsma (VUMC) and Thorsten Böhm (UMCL). We are grateful to Susanne Ziegler (Erlangen) for supporting the acquisitions and in-depth advice. We thank Jacobo Cal Gonzalez (Vienna) for helpful discussions. We thank MIRADA medical (Oxford) for providing us with a research license of their XD software. This study was supported by the European Association of Nuclear Medicine (EANM) covering the travelling costs of Ronald Boellaard and Bernhard Sattler.

Author contributions Protocol/project development: T. Beyer, R. Boellaard, G. Delso, H.H. Quick, B. Sattler. Data collection or management: T. Beyer, R. Boellaard, G. Delso, M.L. Lassen, H.H. Quick, B. Sattler, M. Yaqub. Data analysis: T. Beyer, R. Boellaar, G. Delso, M.L. Lassen, H.H. Quick, B. Sattler, M. Yaqub.

Compliance with ethical standards

Conflict of interest Gaspar Delso is an employee of GE Healthcare and declares no conflict with this manuscript.

Research involving human participants and/or animals All procedures performed in studies involving human participants were in accordance with the ethical standards of the institutional and/or national research committee and with the 1964 Helsinki declaration and its later amendments or comparable ethical standards.

Informed consent Informed consent was obtained from all individual participants included in the study.

References

1. Schmand M, Burbar Z, Corbeil JL et al (2007) BrainPET: first human tomograph for simultaneous (functional) PET and MR imaging. J Nucl Med 48:45
2. Delso G, Fürst S, Jakoby B et al (2011) Performance measurements of the Siemens mMR integrated whole-body PET/MR scanner. J Nucl Med 52:1914–1922
3. Zaidi H, Ojha N, Morich M et al (2011) Design and performance evaluation of a whole-body Ingenuity TF PET-MRI system. Phys Med Biol 56:3091–3106
4. Bailey DL, Barthel H, Beyer T et al (2013) Summary report of the First International Workshop on PET/MR imaging, March 19–23, 2012, Tübingen, Germany. Mol Imaging Biol 15:361–371
5. Bezrukov I, Mantlik F, Schmidt H et al (2013) MR-Based PET attenuation correction for PET/MR imaging. Semin Nucl Med 43:45–59
6. Bailey DL, Barthel H, Beuthien-Baumann B et al (2014) Combined PET/MR: Where are we now? Summary report of the second international workshop on PET/MR imaging April 8–12, 2013, Tubingen, Germany. Mol Imaging Biol 16:295–310
7. Keereman V, Fierens Y, Vanhove C et al (2012) Magnetic resonance-based attenuation correction for micro-single-photon emission computed tomography. Mol Imaging 12:155–165
8. Samarin A, Burger C, Wollenweber SD et al (2012) PET/MR imaging of bone lesions: implications for PET quantification from imperfect attenuation correction. Eur J Nucl Med Mol Imaging 39:1154–1160
9. Keller SH, Holm S, Hansen AE et al (2013) Image artifacts from MR-based attenuation correction in clinical, whole-body PET/MRI. Magn Reson Mater Phy 26:173–181
10. Aznar MC, Sersar R, Saabye J et al (2014) Whole-body PET/MRI: the effect of bone attenuation during MR-based attenuation correction in oncology imaging. Eur J Radiol 83:1177–1183
11. National Electrical Manufacturers Association. NEMA Standards Publication NU 2-2007 (2007) Performance measurements of positron emission tomographs. Rosslyn, VA 26–33
12. EANM Physics Committee, Busemann Sokole E, Płachcínska A et al (2010) Routine quality control recommendations for nuclear medicine instrumentation. Eur J Nucl Med Mol Imaging 37:662–671
13. Boellaard R, O'Doherty MJ, Weber WA et al (2000) FDG PET and PET/CT: EANM procedure guidelines for tumour PET imaging: version 1.0. Eur J Nucl Med Mol Imaging 37:181–200
14. Ziegler S, Braun H, Ritt P et al (2013) Systematic evaluation of phantom fluids for simultaneous PET/MR hybrid imaging. J Nucl Med 54:1464–1471
15. Deller T, Delso G, Grant A, et al (2014) PET NEMA Performance Measurements for a SiPM-Based Time-of-Flight PET/MR System" IEEE Medical Imaging Conference, Seattle #1618
16. Martinez-Möller A, Souvatzoglou M, Delso G et al (2009) Tissue classification as a potential approach for attenuation correction in whole-body PET/MRI: evaluation with PET/CT data. J Nucl Med 50:520–526
17. Boellaard R, Hofman MBM, Hoekstra OS, Lammertsma AA (2014) Accurate PET/MR quantification using time of flight MLAA image reconstruction. Mol Imaging Biol 16(4):469–477
18. Ladefoged CN, Hansen AE, Keller SH (2014) Impact of incorrect tissue classification in Dixon-based MR-AC: fat-water tissue inversion. EJNMMI Phys 1(1):101
19. Schramm G, Langner J, Hofheinz F et al (2013) Quantitative accuracy of attenuation correction in the Philips Ingenuity TF whole-body PET/MR system: a direct comparison with transmission-based attenuation correction. Magn Reson Mater Phy 26(1):115–126
20. Conti M (2011) Why is TOF PET reconstruction a more robust method in the presence of inconsistent data? Phys Med Biol 56(1):155–168
21. Nuyts, J. Michel, M. Fenchel, et al. (2010) Completion of a truncated attenuation image from the attenuated PET emission data. In: IEEE nuclear science symposium conference record 2123–2127
22. Salomon A, Goedicke A, Schweizer B et al (2011) Simultaneous reconstruction of activity and attenuation for PET/MR. IEEE Trans Med Imaging 30:804–813
23. Nuyts J, Bal G, Kehren F et al (2013) Completion of a truncated attenuation image from the attenuated PET emission data. IEEE Trans Med Imaging 32:237–246
24. Blumhagen JO, Ladebeck R, Fenchel M, Scheffler K (2013) MR-based field-of-view extension in MR/PET: B0 homogenization using gradient enhancement (HUGE). Magn Reson Med 70:1047–1057
25. Blumhagen JO, Braun H, Ladebeck R et al (2014) Field of view extension and truncation correction for MR-based human attenuation correction in simultaneous MR/PET imaging. Med Phys. doi:10.1118/1.4861097
26. Hofmann M, Steinke F, Scheel V et al (2008) MRI-based attenuation correction for PET/MRI: a novel approach combining pattern recognition and atlas registration. J Nucl Med 49:1875–1883
27. Hofmann M, Bezrukov I, Mantlik F et al (2011) MRI-based attenuation correction for whole-body PET/MRI: quantitative evaluation of segmentation and atlas based methods. J Nucl Med 52:1392–1399
28. Johansson A, Karlsson M, Nyholm T (2011) CT substitute derived from MRI sequences with ultrashort echo time. Med Phys 38:2708–2714
29. Navalpakkam BK, Braun H, Kuwert T, Quick HH (2013) Magnetic Resonance-based attenuation correction for PET/MR hybrid imaging using continuous valued attenuation maps. Invest Radiol 48:323–332
30. Paulus DH, Quick HH, Geppert C et al (2015) Whole-body PET/MR imaging: quantitative evaluation of a novel model-based MR attenuation correction method including bone. J Nucl Med 56:1061–1066
31. Tellmann L, Quick HH, Bockisch A et al (2011) The effect of MR surface coils on PET quantification in whole-body PET/MR: results from a pseudo-PET/MR phantom study. Med Phys 38:2795–2805
32. Paulus D, Braun H, Aklan B, Quick HH (2011) Simultaneous PET/MR imaging: MR-based attenuation correction of local radiofrequency surface coils. Med Phys 39:4306–4315
33. Kartmann R, Paulus DH, Braun H, Aklan B, Ziegler S, Navalpakkam BK, Lentschig M, Quick HH (2013) Integrated PET/MR imaging: automatic attenuation correction of flexible RF coils. Med Phys. doi:10.1118/1.4812685

34. Wollenweber SD, Delso G, Deller T, Goldhaber D, Hüllner M, Veit-Haibach P (2014) Characterization of the impact to PET quantification and image quality of an anterior array surface coil for PET/MR imaging. Magn Reson Mater Phy 27:149–159
35. Dixon AK (1983) Abdominal fat assessed by computed tomography: sex difference in distribution. Clin Radiol 34:189–191
36. Schramm G, Langner J, Hofheinz F et al (2013) Influence and compensation of truncation artifacts in MR-based attenuation correction in PET/MR. IEEE Trans Med Imaging 32:2056–2063